DOI: 10.1111/cgf.15149
Eurographics Symposium on Rendering 2024
E. Garces and E. Haines
(Guest Editors)

COMPUTER GRAPHICS *forum*
*Volume 43 (2024), Number 4*

# VMF Diffuse: A unified rough diffuse BRDF

Eugene d'Eon and Andrea Weidlich

NVIDIA

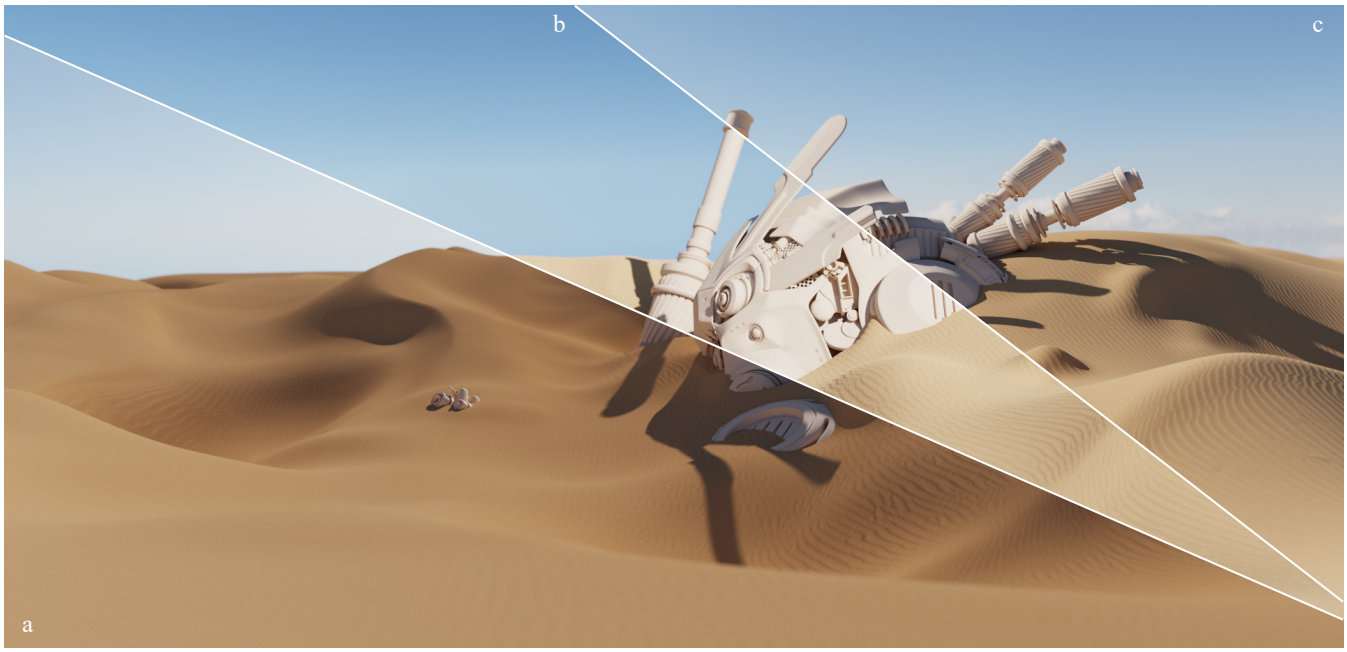


**Figure 1:** *Sand rendered using our new BRDF with illumination from a) the back, b) the front and c) from the side. Both albedo and roughness are constant and set to (0.518,0.331,0.184) and 0.5 respectively. All changes in brightness come from the BRDF itself.*

**Abstract**

*We present a practical analytic BRDF that approximates scattering from a generalized microfacet volume with a von Mises-Fischer NDF. Our BRDF seamlessly blends from smooth Lambertian, through moderately rough height fields with Beckmann-like statistics and into highly rough/porous behaviours that have been lacking from prior models. At maximum roughness, our model reduces to the recent Lambert-sphere BRDF. We validate our model by comparing to simulations of scattering from geometries with randomly-placed Lambertian spheres and show an improvement relative to a rough Beckmann BRDF with very high roughness.*

**CCS Concepts**

• ***Computing methodologies*** → ***Reflectance modeling;***

## 1. Introduction

The accurate representation of diffuse surfaces is pivotal for realistic rendering in computer graphics. While the Lambertian model remains prevalent, its lack of realism has led to the development of more sophisticated alternatives. Notably, the Oren-Nayar model [ON94] is often used due to its simplicity and ease of control. However, this model struggles with granular materials like sand due to the assumption of a Gaussian heightfield. A stochastic evaluation of multiple scattering from diffuse heightfields [HD15] can permit a broader spectrum of behaviours, including anisotropy, and can be

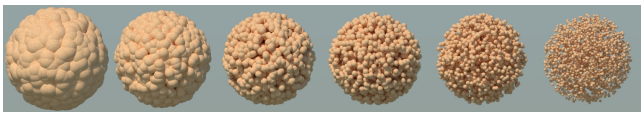

**Figure 2:** *We use Poisson-distributed monodisperse Lambertian spheres as an approximate physical basis for our BRDF. Variation of the sphere radius, while keeping the density fixed, varies the degree of porosity. The roughness parameter of our model is used to navigate this class of stochastic geometry, beginning with Oren-Nayar (heightfield) behaviours (left) when the roughness is low, and transitioning into porous-yet-connected regimes (middle) before exhibiting the Lambert-sphere BRDF (right) at full roughness.*

approximated analytically [Cha18]. However, all heightfield models exhibit unwanted dark artifacts when the roughness is pushed towards the porous regime because the models can only increase roughness by becoming unreasonably spiky [d'E21].

To address these limitations, d'Eon [d'E21] proposed the Lambert-sphere (LS) diffuse BRDF that offers a more granular appearance. However, the underlying physical basis of this model is a dilute suspension of non-intersecting spheres (Figure 2: right), and so does not accurately mimic solid surfaces and is more apt for subsurface scattering in materials like paint. The behavior of *porous-yet-connected* surfaces (Figure 2: middle two images) remains poorly understood and challenging to model with existing BRDFs.

In this paper, we propose to unify all of these diffuse BRDFs into a single intuitive model by using the von Mises-Fischer (vMF) NDF [d'E22] within volumetric microfacet theory [DHd16]. This produces a BRDF with parametric roughness that can continuously blend from Lambertian to Lambert-sphere, with moderate-roughness Beckmann heightfields (similar to Oren-Nayar) in the lower range of roughness values and new porous behaviours in the upper range. For the latter, we compare the predictions of our model to MC simulations of scattering from Poisson-distributed spheres (Figure 2) and find close agreement for roughness values in the porous-yet-connected regime. This provides physical motivation for our model and, to the best of our knowledge, the first confirmation that full-sphere NDFs in *microfacet* (one-sided flake) theory leads to physically-reasonable predictions.

To make our BRDF practical, we first compute reference values using the angular-null-scattering approach [d'E23] and then solve for an approximate analytic form that is reasonably accurate and efficient. Finally, we also include albedo-mapping functions and a roughness parametrization that makes our BRDF intuitive and easy to control.

## 2. Related Work

BSDFs are a fundamental part of rendering systems, and as such, many different forms have been proposed to describe materials. The most popular ones are based on microfacet theory [CT82, vGSK98, WMLT07, Hei14], although many follow the assumption that microfacets are perfectly specular. Contrary to this, Oren and Nayar [ON94] derived a model that is based on Lambertian Gaussian heightfields, which simulates up to two bounces from the surface. A common limitation of these BSDFs is that they cannot model volumetric microgeometry like granular or porous media (Figure 2: middle) where the heightfield assumption is not appropriate.

Anisotropic radiative transfer was introduced to graphics by Jakob et al. [JMA*10] as a two-sided *microflake* theory that can simulate dilute suspensions of oriented scattering particles, which has many applications, such as fabrics [ZJMB11]. The SGGX distribution [HDCD15] is a convenient parametric NDF for describing two-sided flake orientations in such media. Layering slabs of two-sided SGGX flakes has been shown to produce a wide variety of useful behaviours [WJHY22], including approximating heightfield BRDFs. However, the microfacet theory at the heart of most popular BDRFs in graphics fundamentally pertains to heightfields and is therefore best described by a volumetric model with *one-sided* flakes [DHd16], which has been shown to be accurate for both homogeneous and layered configurations [dBWZ23]. To accurately model heightfields in the low-roughness regime, we use one-sided microflakes. However, by choosing an NDF that extends to the full sphere, our model can also describe porous surfaces.

Volumetric scattering in plane-parallel half spaces can also produce diffusive BRDFs [HK93]. A great variety of behaviours can be achieved by varying the phase function and/or varying the medium properties with depth. However, exact solutions are only known for isotropic and linearly-anisotropic phase functions [Cha60]. For phase functions given by three- [HC61] or four-term [Smo76] Legendre expansions, the BRDF takes on a highly complex semi-analytic form that requires specialized fitting procedures to use practically [d'E21]. More general phase functions and layered materials require precomputations using discrete ordinates [Sta01] or adding-doubling [JdJM14].

Various empirical models for diffuse rough surfaces exist. Minnaert [Min41] extended the Lambert BRDF to describe lunar surfaces. Several models have assumed isotropic subsurface scattering and extended Chandrasekhar's BRDF in various forms [Hap81, WNO98]. Burley [Bur12] introduced a BRDF based on measured data which includes a diffuse Fresnel factor. The core assumption of our model is the vMF NDF, which was chosen because it behaves much like the Beckmann NDF for low roughness (to align with Oren-Nayar) and because it approaches an isotropic distribution at full roughness, which recovers the LS BRDF. We employ stochastic geometry, as opposed to measured data, to verify that this choice is physically reasonable (assuming a Lambertian microsurface and geometrical optics).

Recently, [LRPB23] introduced a microfacet model for thin porous layers. Since their model covers sparse granular media only, we consider it orthogonal to our work.

## 3. The vMF Diffuse BRDF

In this section, we propose a new analytic BRDF for rough diffuse materials. Our BRDF has two parameters: $c$ the spectral albedo of the Lambertian microsurface, and a roughness parameter $0 \leq r \leq 1$.

### 3.1. The vMF NDF

To produce a single parametric BRDF that transitions from smooth Lambertian, through moderate-roughness Beckmann and all the way to Lambert-sphere behaviours, we combine microfacet theory with the von Mises-Fischer (vMF) NDF. Unlike Beckmann and GGX NDFs for heightfields, the vMF NDF extends to the full sphere of microfacet orientations. Dupuy et al. [DHd16] noted that the volumetric formulation of Smith microfacet theory (one-sided flakes) requires no fundamental changes to support full-sphere NDFs. However, no practical algorithm for evaluating such BRDFs was presented until recently.

Using a generalization of null-scattering in the angular domain to homogenize the NDF, d'Eon [d'E23] presented an unbiased method to evaluate microfacet BRDFs. This approach supports completely general NDFs (including full-sphere NDFs) and avoids prior requirements to derive cross-sections and sampling procedures for the distribution of visible normals. However, the approach is stochastic and can result in high noise and low performance, depending on the properties of the surface and structure of the input NDF. Therefore, we use this approach only to compute reference values of the target BRDF, and then use this data to fit approximate analytic functions.

#### 3.1.1. Roughness Parametrization

The vMF NDF [GP16, GQGP16], can be defined as [d'E16, d'E22]

$$D^{\mathrm{vMF}}(u) = \frac{\operatorname{csch}\left(\frac{2}{\alpha^2}\right) e^{\frac{2u}{\alpha^2}}}{2\pi\alpha^2} \tag{1}$$

where $u = \cos\theta$ describes the orientation of microfacets, measured from the macroscopic average, and the shape parameter $\alpha > 0$ is chosen such that $D^{\mathrm{vMF}}(u)$ is asymptotic to the Beckmann NDF for small $\alpha$. Note that, unlike the Gaussian NDF for two-sided flakes [ZJMB11], the vMF NDF allows $D(\omega) \neq D(-\omega)$, which is required for making a volume act like a surface [DHd16].

Both the Beckmann and vMF NDFs are valid NDFs for parameter $0 \leq \alpha < \infty$, which is an inconvenient parameter space to texture and control. We found that using a reparametrization

$$\alpha = -\log(1-\sqrt{r}), \quad r \in [0,1], \tag{2}$$

offers a more intuitive mapping using a new roughness variable $r$. This mapping was chosen so that the total diffuse albedo of the BRDF (which is one way to measure how the roughness influences the scattering of light) changes as linearly as possible with $r$.

#### 3.1.2. The vMF Cross Section

In the analytic fitting that we present below, we found that the anisotropic cross section of the vMF NDF was a useful parameter. However, it is known exactly only as an infinite series or as a 1D integral [d'E16]

$$\sigma^{\mathrm{vMF}}(u,\alpha) = \frac{\operatorname{csch}\left(\frac{2}{\alpha^2}\right)}{2\alpha^2} \int_0^1 e^{\frac{2u\sqrt{1-\xi}}{\alpha^2}} {}_0\tilde{F}_1\left(;1;\frac{\xi-\xi u^2}{\alpha^4}\right) \mathrm{d}\xi \tag{3}$$

where ${}_0\tilde{F}_1$ is the regularized confluent hypergeometric function. Therefore, we employ an approximation for $\sigma$ inspired by previous work [d'E16]. For low values of $\alpha$ we use a modification of the Beckmann cross section following d'Eon [d'E16],

$$\begin{aligned}\sigma^{\mathrm{vMF}}(u,\alpha) \approx{}& \frac{1}{4}\left(\tanh\left(\frac{1}{\alpha^2}\right)\left(u-\alpha^2|u|\right)+\left(-\alpha^2-2\right)u+u\coth\left(\frac{1}{\alpha^2}\right)\right)\\ &+\frac{1}{2}\left(u\left(\operatorname{erf}\left(\frac{u}{\alpha\sqrt{1-u^2}}\right)+1\right)+\frac{\alpha\sqrt{1-u^2}e^{\frac{u^2}{\alpha^2\left(u^2-1\right)}}}{\sqrt{\pi}}\right), \quad 0<\alpha<0.25,\end{aligned} \tag{4}$$

which reduces at zero roughness to $\sigma^{\mathrm{vMF}}(u,0) = u\Theta(u)$, using Heaviside's function $\Theta(x)$. For $0.25 < \alpha < 0.9$, a spherical-harmonic expansion of high order can be used [d'E16], or the following

$$\begin{aligned}\sigma^{\mathrm{vMF}}(u,\alpha) \approx{}& 0.25 + (0.4975 - 0.273731(\alpha-0.1)^{1.7})u +\\ &(0.153918 - 0.139522(\alpha-0.1)^{1.2})(3u^2-1) -\\ &(0.013762 + (0.013922\alpha - 0.027553)\alpha)\\ &(3-30u^2+35u^4) + 0.048357\left|(1-\alpha)^4u^8\right| -\\ &0.033493(1-\alpha)^4\cos(7.7u).\end{aligned} \tag{5}$$

For larger $\alpha \geq 0.9$, we use

$$\begin{aligned}\sigma^{\mathrm{vMF}}(u,\alpha) \approx{}& \frac{5}{128}\left(3u^2-1\right)\left(3\alpha^4-6\alpha^2\coth\left(\frac{2}{\alpha^2}\right)+4\right)\\ &-\frac{1}{4}u\left(\alpha^2-2\coth\left(\frac{2}{\alpha^2}\right)\right)+\frac{1}{4},\end{aligned} \tag{6}$$

which has the limit $\sigma^{\mathrm{vMF}}(u,\infty) = 1/4$ for $r = 1$.

### 3.2. Approximation in Fourier Space

Our BRDF can be stochastically evaluated using the angular-null-scattering method [d'E23] by combining the vMF NDF (Equation 1) with one-sided Lambertian flakes. This approach becomes prohibitively costly for all but very large roughness values, due to the rejection sampling in the null algorithm. Therefore, we precomputed a set of reference evaluations of our BRDF and then fit analytic functions to that data to define an approximate parametric model.

We employ a decomposition of the BRDF over scattering order, similar to Oren and Nayar [ON94], in order to reduce the dimensionality of the functions that require approximation. Where Oren

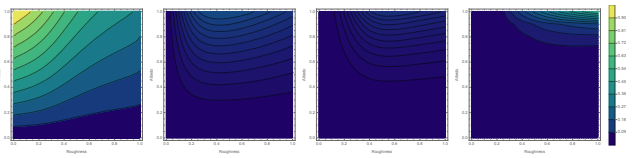

**Figure 3:** *Energy contribution of each component with varying albedo and roughness. While the majority of the energy is accounted for in the single scattering, for materials with high albedo and high roughness a significant amount of the energy is present in $f_m$.*

and Nayar include two orders of scattering, we include a large number to ensure that the highly porous regime does not lose energy. The BRDF is then written as

$$f_r(\vec{\omega}_i,\vec{\omega}_o) = c f_1(\vec{\omega}_i,\vec{\omega}_o) + c^2 f_2(\vec{\omega}_i,\vec{\omega}_o) + c^3 f_3(\vec{\omega}_i,\vec{\omega}_o) + f_{\mathrm{m}}(\vec{\omega}_i,\vec{\omega}_o), \tag{7}$$

where $f_{\mathrm{m}}(\vec{\omega}_i,\vec{\omega}_o)$ includes fourth- and higher-order scattering from the surface. The contribution of each component can be seen in Figure 3.

An additional dimensionality reduction is gained by using a Fourier expansion, similar to the Lambert-sphere BRDF [d'E21]. For the first three scattering orders, and for each pair of incoming and outgoing cosines ($u_{\mathrm{i}} = \cos\theta_i, u_{\mathrm{o}} = \cos\theta_o$), we computed azimuthal integrals of the BRDF and expressed each using a discrete cosine series over azimuth $\phi$

$$f_i(\vec{\omega}_i,\vec{\omega}_o) \approx f_i^{(0)}(u_{\mathrm{i}},u_{\mathrm{o}}) + f_i^{(1)}(u_{\mathrm{i}},u_{\mathrm{o}})\cos(\phi) + f_i^{(2)}(u_{\mathrm{i}},u_{\mathrm{o}})\cos(2\phi).$$

Noting that negligible energy is present in higher order components of the expansion, an accurate analytic form of the first three bounces from the microsurface is achieved when the functions $f_i^{(j)}(u_{\mathrm{i}},u_{\mathrm{o}})$ are all accurately approximated. Having removed dependence on azimuth $\phi$ and albedo $c$, these functions are functions of only three parameters $(u_{\mathrm{i}},u_{\mathrm{o}},r)$.

For the specific approximations that follow, we took inspiration from the functional forms that appeared in the exact solution for the Lambert-sphere BRDF. Since this BRDF appears as a special case of our new BRDF, it seemed likely that a similar computational complexity (with similar functions appearing) would likely be required to accurately fit the reference data.

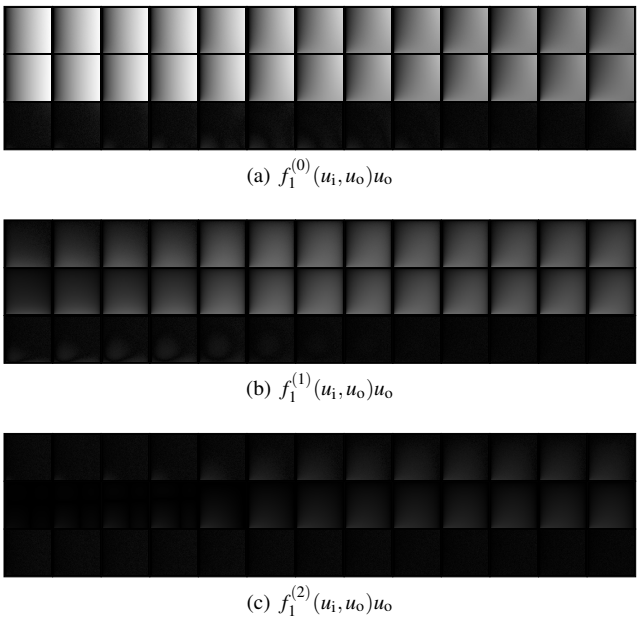

(a) $f_1^{(0)}(u_{\mathrm{i}},u_{\mathrm{o}})u_{\mathrm{o}}$

(b) $f_1^{(1)}(u_{\mathrm{i}},u_{\mathrm{o}})u_{\mathrm{o}}$

(c) $f_1^{(2)}(u_{\mathrm{i}},u_{\mathrm{o}})u_{\mathrm{o}}$

**Figure 4:** *MC Reference (top) vs approximate (middle) Fourier components of $f_1(\vec{\omega}_i,\vec{\omega}_o)*\cos\theta_o$ for single scattering. Error (bottom) shows a close match over a range of roughness values and pairs of cosines. Each square shows $u_o \in [0,1]$ on the horizontal and $u_i \in [0,1]$ on the vertical, with $u_i = u_o = 1$ in the top right corner. The roughness values from left to right are $r \in \{0.025, 0.05, 0.075, 0.1, 0.2, 0.3, 0.4, 0.5, 0.6, 0.7, 0.8, 0.9, 1\}$.*

Each approximation that follows was found by trial and error by searching for a parametric form with as few coefficients as possible showing low error over a wide range of roughnesses. This was judged visually by comparing the Fourier coefficients over a fixed set of roughnesses and displaying both reference and fitted values together with a difference image. For each component, we attempted to find the simplest equation that did not show noticeable error in the difference image (e.g. Figure 4). However, it may be possible that simpler expressions could accurately describe our BRDF.

Once a low-error form was selected, simple approximate functions for the coefficients as a function of roughness were fit using simple expressions. While these expressions offer little direct insight on their own, it is interesting to note the similarities to some expressions appearing in the simpler special case of the Lambert-sphere.

### 3.3. First-Order Collision

For rays that intersect the surface exactly once, we observed that the zeroth-order Fourier component is well approximated by

$$f_1^{(0)}(u_{\mathrm{i}},u_{\mathrm{o}}) \approx \frac{1}{\pi}\frac{\sigma^{\mathrm{vMF}}(u_{\mathrm{i}})\sigma^{\mathrm{vMF}}(u_{\mathrm{o}})}{u_{\mathrm{i}}\sigma^{\mathrm{vMF}}(-u_{\mathrm{o}}) + u_{\mathrm{o}}\sigma^{\mathrm{vMF}}(u_{\mathrm{i}})} \times \left(C_{100} + C_{101}u_{\mathrm{i}}u_{\mathrm{o}} + C_{102}u_{\mathrm{i}}^2u_{\mathrm{o}}^2 + C_{103}(u_{\mathrm{i}}^2+u_{\mathrm{o}}^2)\right),$$

$$C_{100} = 1 + \frac{0.84r^4 - 0.1r}{9r^3+1}, \quad C_{101} = \frac{-9.47r^3 + 20.4r^2 + 0.0173r}{7.46r+1},$$

$$C_{102} = \frac{2.37r^2 - 0.927r}{r^2+1.24}, \quad C_{103} = \frac{-1.54r^2 - 0.11r}{7.1r^2 - 1.05r + 1}.$$

The term involving the cross sections was inspired by considering single-scattering from a medium with angle-dependent cross-section, integrating over all depths in a half space to find

$$\frac{1}{u_{\mathrm{i}}u_{\mathrm{o}}}\int_0^\infty \mathrm{e}^{-z\sigma(-u_{\mathrm{i}})/u_{\mathrm{i}}}\mathrm{e}^{-z\sigma(u_{\mathrm{o}})/u_{\mathrm{o}}}dz = \frac{1}{u_{\mathrm{i}}\sigma(-u_{\mathrm{o}}) + u_{\mathrm{o}}\sigma(u_{\mathrm{i}})}. \tag{8}$$

For the first-order component, we propose the approximation

$$f_1^{(1)}(u_{\mathrm{i}},u_{\mathrm{o}}) \approx \frac{1}{\pi}\frac{[\sigma^{\mathrm{vMF}}(u_{\mathrm{i}})\sigma^{\mathrm{vMF}}(u_{\mathrm{o}})]^{C_{112}}}{u_{\mathrm{i}}\sigma^{\mathrm{vMF}}(-u_{\mathrm{o}}) + u_{\mathrm{o}}\sigma^{\mathrm{vMF}}(u_{\mathrm{i}})}\sqrt{1-u_{\mathrm{i}}^2}\sqrt{1-u_{\mathrm{o}}^2} \times (C_{110} + C_{111}u_{\mathrm{i}}u_{\mathrm{o}}),$$

$$C_{110} = \frac{0.54r - 0.182r^3}{1.32r^2+1}, \quad C_{111} = \frac{-0.375r^3 + 0.62r^2 - 0.097r}{0.4r^3+1}$$

$$C_{112} = -0.681r^2 + 0.862r + 0.283.$$

For the second-order component, we propose the approximation

$$f_1^{(2)}(u_{\mathrm{i}},u_{\mathrm{o}}) \approx \frac{\left(1-u_{\mathrm{i}}^2\right)\left(1-u_{\mathrm{o}}^2\right)(C_{120}+C_{121}u_{\mathrm{i}})(C_{120}+C_{121}u_{\mathrm{o}})}{\pi(u_{\mathrm{i}}+u_{\mathrm{o}})},$$

$$C_{120} = \frac{5.1r^2 + 2.25r}{32.4r^2 + 9.8r + 1}, \quad C_{121} = \frac{6r^3 - 4.32r}{287r^3 + 9.7r + 1}.$$

The accuracy of these three approximations is illustrated in Figure 4. Note that for $r = 0$, all but $C_{100} = 1$ go to zero and Lambertian

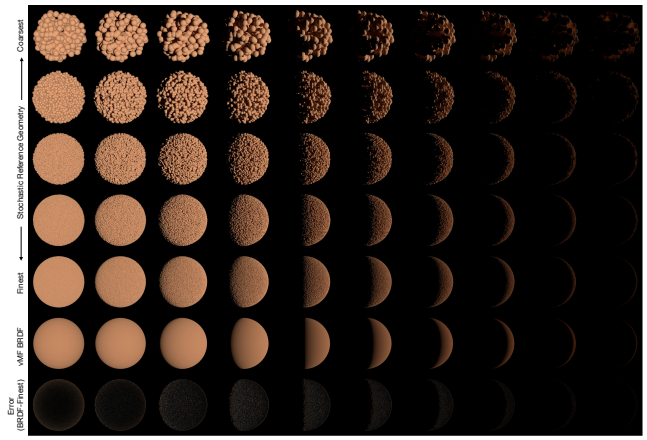


(a) roughness $r = 0.5$

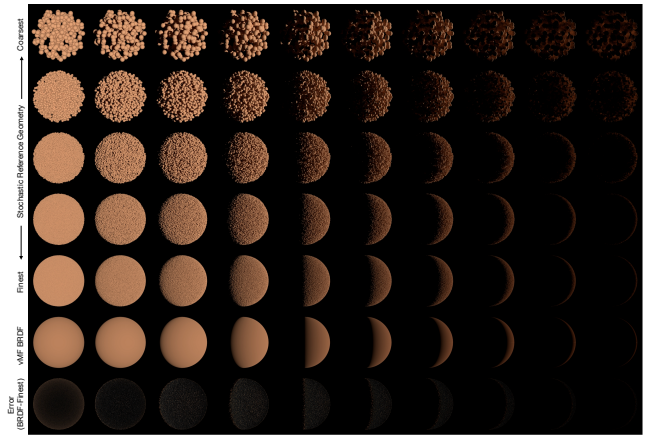


(b) roughness $r = 0.6$

**Figure 5:** *Comparison of stochastic geometry (top rows) to our BRDF prediction (second last row), with an error image (bottom row which subtracts the BRDF and finest-level reference), for two roughness values in the porous-yet-connected regime. With the exception of the hot-spot effect shown on the left column, which is not predicted by our model, note the low error between our BRDF and ground truth for a variety of lighting directions.*

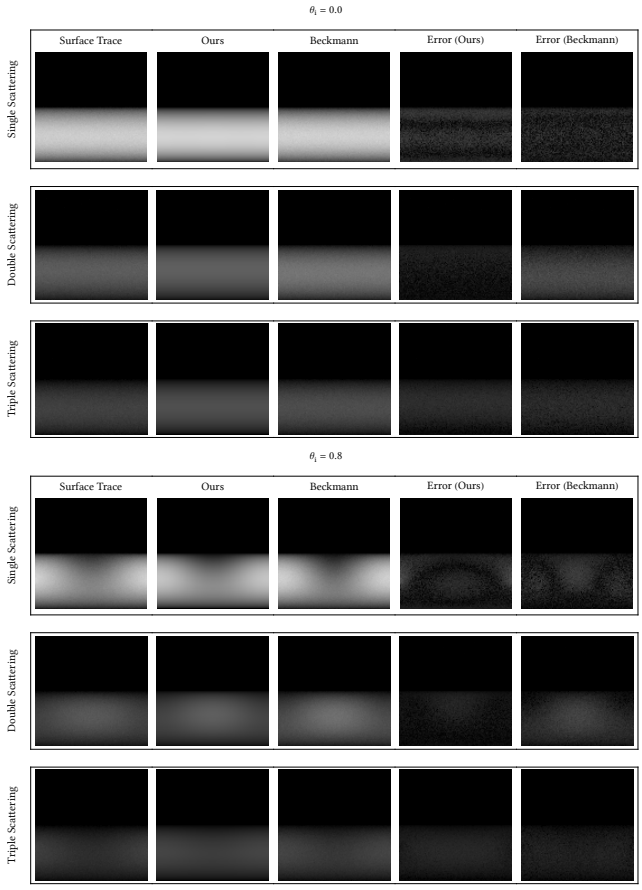


**Figure 6:** *Comparison of the hemispherical reflectance of stochastic geometry ("surface trace") to our BRDF (with $r = 0.4$) and a Beckmann heightfield model (with roughness $\alpha = 1.4$) for fixed incoming angle $\theta_i$. Note how for the second bounce the heightfield model over-predicts the reflectance, where our porous BRDF exhibits lower error.*

behaviour is recovered exactly (noting also that $\sigma^{\mathrm{vMF}}(u) \to u\Theta(u)$ as $\alpha \to 0$, where $\Theta$ is Heaviside's function).

For the higher-order terms, the same approach was taken and expressions of similar complexity appear. We include these in Appendix A.

## 4. Validation

To provide physical motivation for our BRDF, we performed brute-force MC simulation of parallel light rays reflecting from an ensemble of stochastic geometries and compared the results to our BRDF. We chose Poisson-distributed monodisperse spheres, where variation of the radius induces a variation in roughness (see Figure 2). This class of geometry was chosen because it is efficient to sample from and because it interpolates between the two roughness extremes of our BRDF: in the limit of infinite radius, the geometry approaches a flat Lambertian material, and as the radius becomes small, the geometry becomes a dilute suspension of non-intersecting Lambert spheres, which aligns exactly with the Lambert-sphere BRDF [d'E21]). More importantly, this geometry can exhibit porous (yet connected) ensembles and provides the first test bed for verifying that the extension of microfacet theory to include full-sphere NDFs produces physically meaningful results.

In Figure 5 we compare renders of explicit stochastic geometry and our BRDF, with error images in the bottom row. The top rows show a sequence of stochastic geometries that use successively smaller spheres, while maintaining a fixed ratio of radius to density. In the limit of zero radius, the spheres becomes too small to resolve and the result approaches that of a BRDF applied to a single sphere shape. Our BRDF is shown next to the finest level of geometry. For these two roughness levels, where the geometry shows distinct porosity, yet appears mostly connected, we see a low

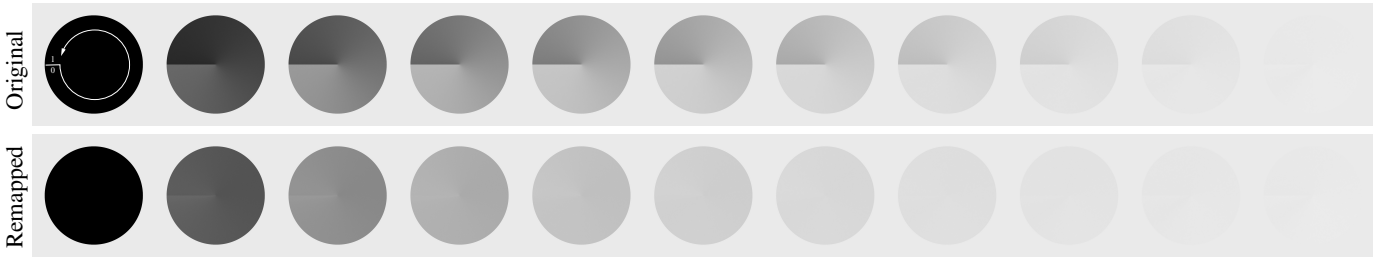


**Figure 7:** *Comparison of original (top) and remapped albedo (bottom) rendered on a sphere in a white IBL. The roughness changes from 0 to 1 counterclockwise. The albedo of each sphere is constant and increases from left to right.*

**Figure 8:** *Light spin around an object with a roughness texture with values ranging from 0 to 1. Different patches flare up at different times.*

error between our BRDF and the ground truth (except for the left column where the light and camera are aligned perfectly, which produces the well known hotspot effect that is not accounted for in microfacet theory).

In Figure 6 we compare two hemispherical slices of our BRDF under fixed $\theta_i$ illumination to ensemble-averaged reflectance from thick slabs of random sphere geometry (like that shown in Figure 2). Additional slices are provided in the supplemental material. For both our model and a diffuse Beckmann heightfield [HD15], we manually determined roughnesses that approximately minimized the observed error for the single-scattering component of the reflectance. Note how for the second surface bounce that our BRDF has lower error than the heightfield model. Considering these results together with Figure 5, we conclude that using the vMF NDF in full-sphere microfacet theory is not simply a convenient mathematical choice for interpolating between prior models but also a physically-plausible BRDF for porous diffuse microgeometries.

## 5. Albedo Correction

One side-effect of considering multiple bounces is that with increasing roughness, materials will become darker and more saturated due to absorption (e.g., see 3rd row of Figure 10). This behaviour is physically correct and has been observed for scattering from rough heightfields [HD15]. This may be a desirable behaviour when varying the roughness over a surface that has uniform absorption. However, it can make dialing in a desired color difficult. For this reason, we provide an optional color re-mapping function that solves for the unique diffuse albedo $c$ of the microsurface that produces a diffuse albedo $k_\mathrm{d}$ (assuming normal incidence),

$$c = \left( \frac{-1 + k_\mathrm{d} + \sqrt{1 - 2k_\mathrm{d} + k_\mathrm{d}^2 + 4s^2 k_\mathrm{d}^2}}{2sk_\mathrm{d}} \right) \sqrt{r} + (1.0 - \sqrt{r}) k_\mathrm{d}$$

with $s = 0.64985 + 0.631112r + 1.38922r^2$. Figure 7 shows the effect of our remapping.

## 6. Results

We implemented our BRDF in Mitsuba 0.6 [Jak10]. A video of a scene with 1M triangles and a rotating light is provided in the supplemental material. It shows the behaviour of our model with porous-yet-connected roughness ($r = 0.5$). For this scene, we observed no measurable performance difference compared to rendering with the full Oren-Nayar BRDF.

Figure 1 shows our BRDF applied to sand rendering under a variety of illumination directions. Note how the brightness changes under different viewing directions. To demonstrate this further, we rendered an object with a roughness texture with different lighting directions. Although we apply our remapping scheme and all textures have more or less the same albedo, different patches flare up in different lighting configurations appearing brighter and darker (Figure 8).

As it can be seen in Figure 10, while Oren-Nayar and our model are identical at $r = 0$ and similar at low roughness, they start to diverge when the roughness is increased. Notably, both the full as well as the approximative Oren-Nayar model will not conserve energy and become darker since it only models two bounces. In contrast, our model will preserve energy, and exhibit increased darkening and saturation due to absorption during subsequent bounces. However, the albedo can be remapped so that the color stays approximately constant. At $r = 1$, our model closely approximates the LS BRDF (albeit with less accuracy than the original approximation [d'E21]).

While our model simulates only purely diffuse materials, it can

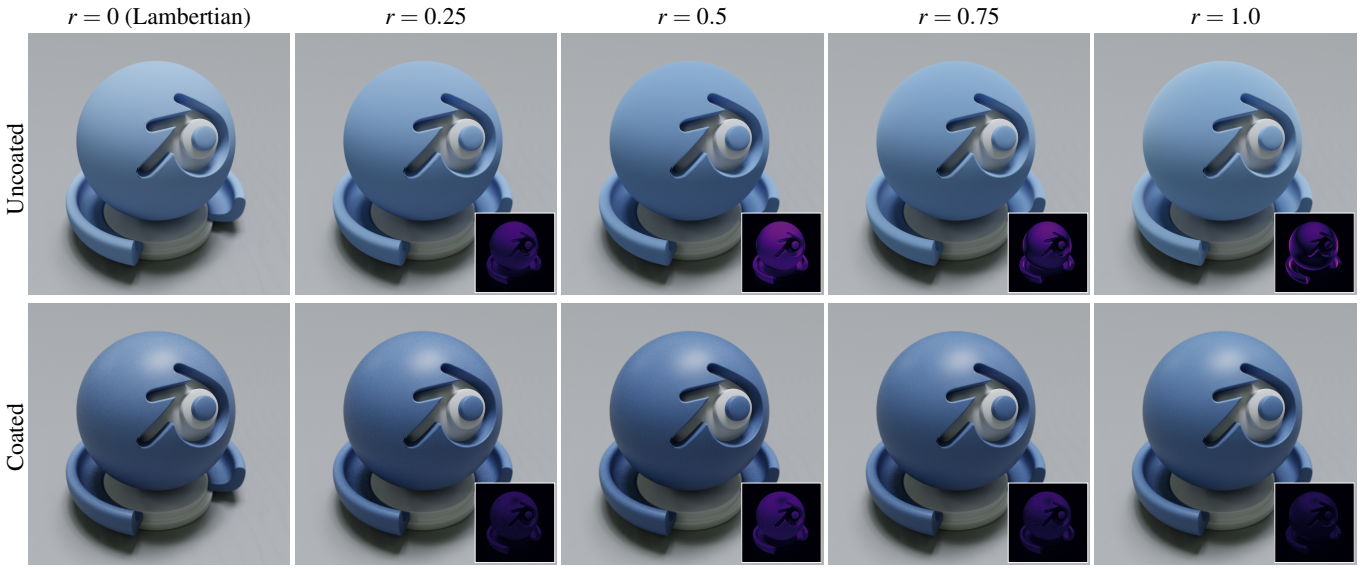


**Figure 9:** *When coated with a dielectric specular BSDF, our diffuse BRDF loses its typical bright edges. The appearance difference to the Lambertian base ($r = 0$) can be seen in the small ꟻLIP [ANA*20] image. As it can be seen, the visual difference stays comparatively constant when coated whereas the grazing angles change significantly in the uncoated case if the roughness is increased.*

be combined with specular BSDFs to simulate materials like ceiling paint or sand. In Figure 9, we coated our vMF diffuse BRDF with a GGX BSDF with IOR 1.4 using [GHZ18]'s method and increased the roughness of the base layer from 0.0 to 1.0 with remapping enabled. While grazing angles vary significantly in the uncoated case, the effect diminishes when coated since the refracted rays approach the diffuse base from a narrower range than in the case of no coating. Note that our remapping only takes into account the color-change from the roughness. The darkening of the coated versions is caused by the scattering between top and base layer. For each image, we include a difference image that compares to the first (Lambertian base) image to show that the roughness variation in our model can still be visually significant behind a rough dielectric coating.

## 7. Conclusions

We have presented a new analytic BRDF that models a wide variety of diffuse behaviours, including several important prior models as special cases. It is easy to use and has been compared to ground truth simulation, showing a close comparison, and an improved accuracy for porous microgeometries when compared to heightfield BRDFs .

Our BRDF has certain limitations. We do not support anisotropy or perfect importance sampling. Instead, we currently rely on Lambertian sampling. In practice, the shape of the BRDF is uniform enough that the additional noise is not prohibitive.

Since our BRDF is not as simple as, for example, Oren-Nayar or other empirical models and involves many computations, it is mainly suited for offline rendering. However, due to its closed-form solution and its small set of parameters, it is likely that our BRDF could be accurately approximated by a small Multi-Layer Perceptron (MLP) for use in real-time rendering [ZRW*24].

## Acknowledgements

The material test blob in Figure 8, Figure 9 and Figure 10 was created by Robin Marin and released under creative commons license.

## Appendix A: Additional Approximations

### Second-Order Collision

For rays that intersect the surface exactly twice, we observed that the zeroth-order Fourier component is well approximated by

$$f_2^{(0)}(u_\mathrm{i},u_\mathrm{o}) \approx \frac{\left(C_{200}+C_{201}u_\mathrm{i}u_\mathrm{o}+C_{202}(u_\mathrm{i}+u_\mathrm{o})+C_{203}u_\mathrm{i}^2u_\mathrm{o}^2+C_{204}(u_\mathrm{i}^2+u_\mathrm{o}^2)\right)}{\pi(u_\mathrm{i}+u_\mathrm{o})},$$

$$C_{200}=\frac{0.226r^2+0.00056r}{7.07r^2+1},\quad C_{201}=\frac{-12.04r^3+4.57r^2-0.268r}{36.7r^3+1},$$

$$C_{202}=\frac{-0.97r^3+2.52r^2+0.418r}{10r^2+1},\quad C_{203}=\frac{2.65r^3-2.25r^2+0.068r}{21.4r^3+1},$$

$$C_{204}=\frac{0.05r-4.22r^3}{43.1r^3+17.6r^2+1}.$$

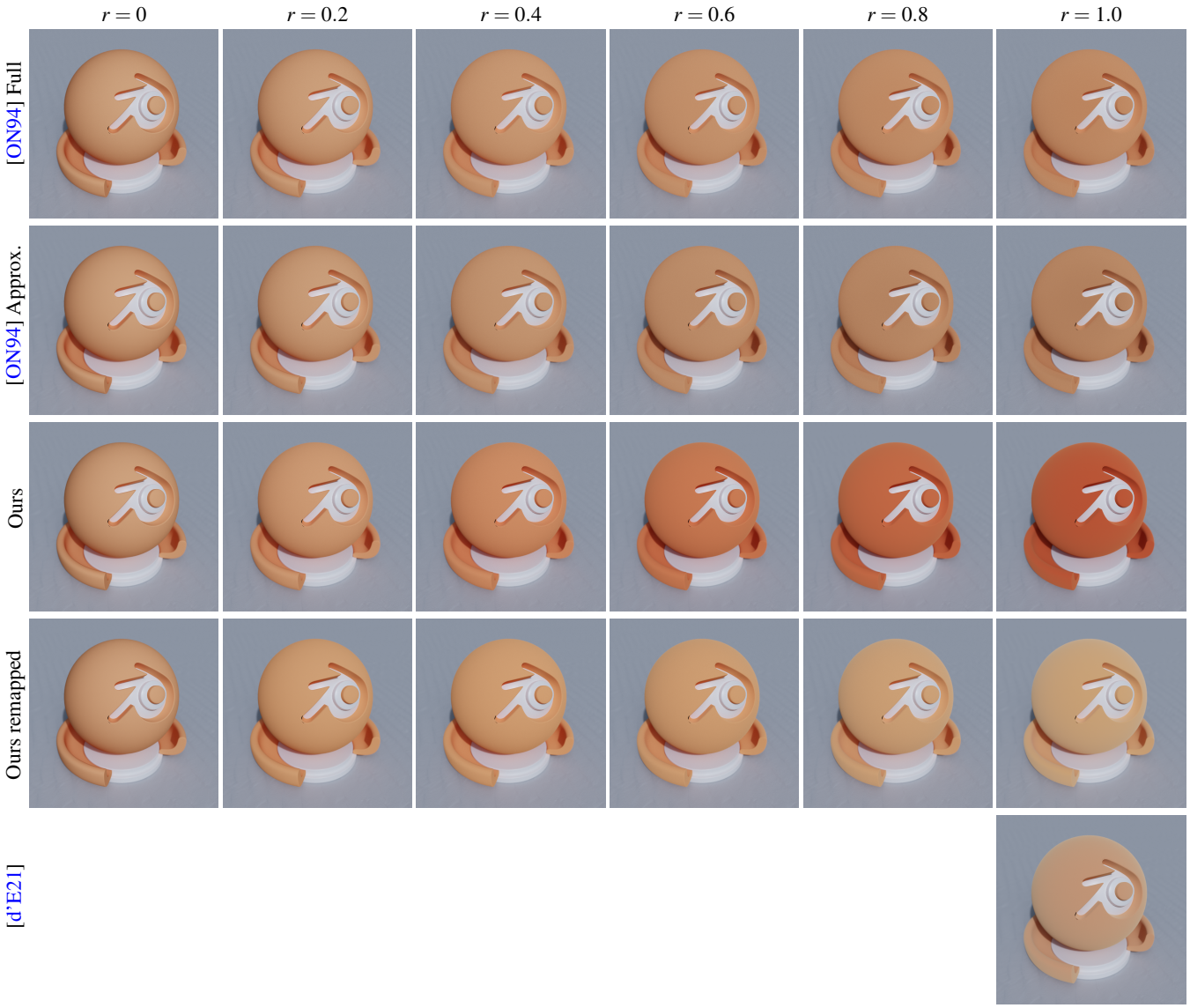


**Figure 10:** *Comparison of Oren-Nayar vs. our model. The albedo of all spheres is (0.9,0.4,0.2). With increasing roughness, saturation starts to increase. We can compensate the darkening and saturation increase with our remapping to allow for easier editing.*

For the first-order component, we propose

$$f_2^{(1)}(u_\mathrm{i},u_\mathrm{o}) \approx \frac{1}{\pi}\frac{\sqrt{1-u_\mathrm{i}^2}\sqrt{1-u_\mathrm{o}^2}}{u_\mathrm{i}+u_\mathrm{o}} \times \left(C_{210}+C_{211}u_\mathrm{i}u_\mathrm{o}+C_{212}(u_\mathrm{i}+u_\mathrm{o})\right),$$

$$C_{210} = \frac{-0.027r^3-0.049r}{3.36r^2+1}, \quad C_{211} = \frac{-8.332r^{2.5}+6.073r^3+2.77r^2}{50r^4+1},$$

$$C_{212} = \frac{-0.295r^3-0.431r^2}{23.9r^3+1}.$$

We observed negligible energy in the second- and higher-order components of the second bounce and assume these are zero in our approximations ($f_2^{(2+)}(u_\mathrm{i},u_\mathrm{o}) = 0$). Our approximations are compared to MC reference in Figure 11. Because all constants $C_{2ij} = 0$ when $r = 0$, no second-order energy arises and the Lambertian BRDF is recovered exactly.

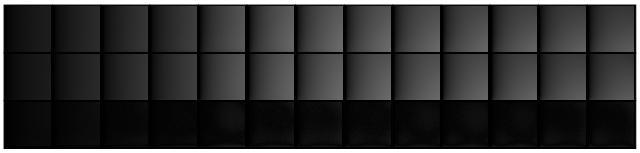

(a) $f_2^{(0)}(u_\mathrm{i},u_\mathrm{o})u_\mathrm{o}$

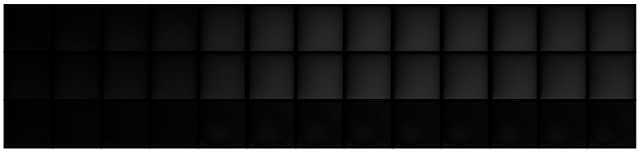

(b) $f_2^{(1)}(u_\mathrm{i},u_\mathrm{o})u_\mathrm{o}$

**Figure 11:** *Reference (top) vs approximate (middle) Fourier components of $f_2(\vec{\omega}_i,\vec{\omega}_o)*\cos\theta_o$ for double scattering. Error (bottom) shows a close match over a range of roughness values and pairs of cosines.*

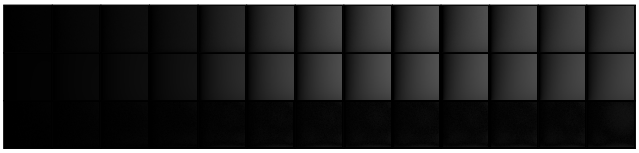

(a) $f_3^{(0)}(u_\mathrm{i},u_\mathrm{o})u_\mathrm{o}$

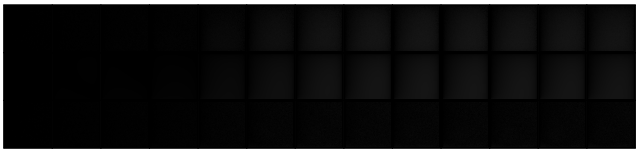

(b) $f_3^{(1)}(u_\mathrm{i},u_\mathrm{o})u_\mathrm{o}$

**Figure 12:** *Reference (top) vs approximate (middle) Fourier components of $f_3(\vec{\omega}_i,\vec{\omega}_o)*\cos\theta_o$ for triple scattering. Error (bottom) shows a close match over a range of roughness values and pairs of cosines.*

### Third-Order Collision

For rays that intersect the surface exactly three times, we observed that the zeroth-order Fourier component is well approximated by

$$f_3^{(0)}(u_\mathrm{i},u_\mathrm{o}) \approx \frac{\left(C_{300}+C_{301}u_\mathrm{i}u_\mathrm{o}+C_{302}(u_\mathrm{i}+u_\mathrm{o})+C_{303}u_\mathrm{i}^2u_\mathrm{o}^2+C_{304}(u_\mathrm{i}^2+u_\mathrm{o}^2)\right)}{\pi(u_\mathrm{i}+u_\mathrm{o})},$$

$$C_{300}=\frac{0.262r^4-0.083r^3}{38.6r^4-1.9r^2+1},\quad C_{301}=\frac{4.95r^{2.5}-2.44r^3-0.627r^2}{31.5r^4+1}$$

$$C_{302}=\frac{0.31r^{2.5}+1.4r^3+0.33r^2}{20r^3+1},C_{303}=\frac{1.77r^{2.5}-4.06r^3-0.74r^2}{215r^5+1},$$

$$C_{304}=-\frac{1.026r^3}{13.2r^3+5.81r^2+1}.$$

For the first-order component, we propose

$$f_3^{(1)}(u_\mathrm{i},u_\mathrm{o}) \approx \frac{1}{\pi}\frac{\sqrt{1-u_\mathrm{i}^2}\sqrt{1-u_\mathrm{o}^2}}{u_\mathrm{i}+u_\mathrm{o}}\times \left(C_{310}+C_{311}u_\mathrm{i}u_\mathrm{o}+C_{312}(u_\mathrm{i}+u_\mathrm{o})\right),$$

$$C_{310}=\frac{0.028r^2-0.0132r^3}{-3.315r^4+7.46r^2+1},C_{311}=\frac{0.162r^{2.5}+0.302r^3-0.134r^2}{57.5r^{4.5}+1},$$

$$C_{312}=\frac{0.5r^{2.5}-0.207r^3-0.119r^2}{18.7r^3+1}.$$

We observed negligible energy in the second- and higher-order components of the third bounce and assume these are zero in our approximations ($f_3^{(2+)}(u_\mathrm{i},u_\mathrm{o})=0$). Our approximations are compared to MC reference in Figure 12. Lambertian behaviour follows, like before, noting $C_{3ij}=0$ when $r=0$.

### Higher-Order Scattering

For rays that scatter four or more times from the microsurface, we propose an analytic approximation that was found using TuringBot symbolic regression software,

$$f_\mathrm{m}(\vec{\omega}_i,\vec{\omega}_o) = 0.384C_k(C_a-0.342)C_a\left(|\tanh(r)-0.09|-\frac{0.0579}{u_\mathrm{i}u_\mathrm{o}+0.288}\right),$$

$$C_k=\frac{-0.453(1-c)-0.544\sqrt{1-c}+1}{1.429\sqrt{1-c}+1},$$

$$C_a=c\left(1.169\sqrt{1-c}+1\right)^{-\tan^{-1}\left(((r-0.265)r+0.0225)\mathrm{erf}\left(\sqrt{1-c}\right)\right)}. \quad (9)$$

### References


[ANA*20] ANDERSSON P., NILSSON J., AKENINE-MÖLLER T., OSKARSSON M., ÅSTRÖM K., FAIRCHILD M. D.: ꟻLIP: A Difference Evaluator for Alternating Images. *Proceedings of the ACM on Computer Graphics and Interactive Techniques 3*, 2 (2020), 15:1–15:23. doi:10.1145/3406183. 7

[Bur12] BURLEY B.: Physically-based shading at disney. In *ACM SIGGRAPH 2012 Courses* (2012), ACM, Association for Computing Machinery, pp. 1–7. 2

[Cha60] CHANDRASEKHAR S.: *Radiative Transfer*. Dover, 1960. 2

[Cha18] CHAN D.: Material advances in Call of Duty: WWII. In *ACM SIGGRAPH 2018 Courses* (2018), SIGGRAPH '18, Association for Computing Machinery. URL: https://doi.org/10.1145/3214834.3264541, doi:10.1145/3214834.3264541. 2

[CT82] COOK R. L., TORRANCE K.: A reflectance model for computer graphics. In *ACM Transactions on Graphics (TOG)* (1982), pp. 7–24. URL: https://doi.org/10.1145/357290.357293. 2

[dBWZ23] D'EON E., BITTERLI B., WEIDLICH A., ZELTNER T.: Microfacet theory for non-uniform heightfields. *ACM Transactions on graphics (TOG)* (2023), 1–10. URL: https://doi.org/10.1145/3588432.3591486. 2

[d'E16] D'EON E.: *The anisotropic cross-section for the spherical Gaussian medium*. Tech. rep., 2016. URL: https://eugenedeon.com/pdfs/sgcross.pdf. 3

[d'E21] D'EON E.: An analytic brdf for materials with spherical lambertian scatterers. *Computer Graphics Forum 40*, 4 (2021), 153–161. URL: https://doi.org/10.1111/cgf.14348. 2, 4, 5, 6, 8

[d'E22] D'EON E.: *A Hitchhiker's Guide to Multiple Scattering*, 0.3.2.0 ed. Self Published, 2022. URL: https://eugenedeon.com/hitchhikers. 2, 3

[d'E23] D'EON E.: Student-T and beyond: Practical tools for multiple-scattering bsdfs with general NDFs. In *ACM SIGGRAPH 2023 Talks*. 2023, pp. 1–2. URL: https://research.nvidia.com/labs/rtr/student-beyond/. 2, 3

[DHd16] DUPUY J., HEITZ E., D'EON E.: Additional progress towards the unification of microfacet and microflake theories. In *EGSR (EI&I)* (2016), pp. 55–63. URL: http://dx.doi.org/10.2312/sre.20161210. 2, 3

[GHZ18] GUO Y., HAŠAN M., ZHAO S.: Position-free monte carlo simulation for arbitrary layered bsdfs. *ACM Transactions on Graphics (TOG) 37*, 6 (Dec. 2018). URL: https://doi.org/10.1145/3272127.3275053, doi:10.1145/3272127.3275053. 7

[GP16] GUO J., PAN J.-G.: Real-time rendering of refracting transmissive objects with multi-scale rough surfaces. *The Visual Computer 32* (2016), 1579–1592. URL: https://doi.org/10.1007/s00371-015-1141-8. 3

[GQGP16] GUO J., QIAN J., GUO Y., PAN J.: Rendering thin transparent layers with extended normal distribution functions. *IEEE Transactions on Visualization and Computer Graphics 23*, 9 (2016), 2108–2119. URL: https://doi.org/10.1109/TVCG.2016.2617872. 3

[Hap81] HAPKE B.: Bidirectional reflectance spectroscopy: 1. theory. *Journal of Geophysical Research: Solid Earth 86*, B4 (1981), 3039–3054. doi:https://doi.org/10.1029/JB086iB04p03039. 2

[HC61] HORAK H. G., CHANDRASEKHAR S.: Diffuse reflection by a semi-infinite atmosphere. *Astrophys. J. 134* (July 1961), 45. doi:10.1086/147126. 2

[HD15] HEITZ E., DUPUY J.: *Implementing a simple anisotropic rough diffuse material with stochastic evaluation*. Tech. rep., 2015. URL: https://eheitzresearch.wordpress.com/research/. 1, 6

[HDCD15] HEITZ E., DUPUY J., CRASSIN C., DACHSBACHER C.: The SGGX microflake distribution. *ACM Transactions on Graphics (TOG) 34*, 4 (July 2015). URL: https://doi.org/10.1145/2766988, doi:10.1145/2766988. 2

[Hei14] HEITZ E.: Understanding the masking-shadowing function in microfacet-based brdfs. *Journal of Computer Graphics Techniques 3*, 2 (2014), 32–91. URL: http://jcgt.org/published/0003/02/03/. 2

[HK93] HANRAHAN P., KRUEGER W.: Reflection from layered surfaces due to subsurface scattering. In *Proceedings of ACM SIGGRAPH 1993* (1993), pp. 164–174. URL: https://doi.org/10.1145/166117.166139. 2

[Jak10] JAKOB W.: Mitsuba renderer, 2010. http://www.mitsuba-renderer.org. 6

[JdJM14] JAKOB W., D'EON E., JAKOB O., MARSCHNER S.: A comprehensive framework for rendering layered materials. *ACM Transactions on Graphics (ToG) 33*, 4 (2014), 1–14. URL: https://doi.org/10.1145/2601097.2601139. 2

[JMA*10] JAKOB W., MOON J. T., ARBREE A., BALA K., MARSCHNER S.: A radiative transfer framework for rendering materials with anisotropic structure. *ACM Transactions on Graphics (TOG) 29*, 10 (July 2010), 53:1–53:13. doi:10.1145/1778765.1778790. 2

[LRPB23] LUCAS S., RIBARDIERE M., PACANOWSKI R., BARLA P.: A micrograin bsdf model for the rendering of porous layers. In *SIGGRAPH Asia 2023 Conference Papers* (2023), Association for Computing Machinery. URL: https://doi.org/10.1145/3610548.3618241, doi:10.1145/3610548.3618241. 2

[Min41] MINNAERT M.: The reciprocity principle in lunar photometry. *Astrophysical Journal, vol. 93, p. 403-410 (1941). 93* (1941), 403–410. 2

[ON94] OREN M., NAYAR S. K.: Generalization of lambert's reflectance model. In *SIGGRAPH* (1994), SIGGRAPH '94, Association for Computing Machinery, p. 239–246. URL: https://doi.org/10.1145/192161.192213, doi:10.1145/192161.192213. 1, 2, 3, 8

[Smo76] SMOKTIY O.: Exact solution of a problem of diffuse reflection of solar radiation by a semiinfinite planetary atmosphere with a four-term scattering phase function. *Izvestiya, Atmospheric and Oceanic Physics 12*, 10 (1976), 1053–1066. 2

[Sta01] STAM J.: An illumination model for a skin layer bounded by rough surfaces. In *Rendering Techniques (Proc. EG Symposium on Rendering)* (2001), pp. 39–52. URL: https://doi.org/10.1007/978-3-7091-6242-2_4. 2

[vGSK98] VAN GINNEKEN B., STAVRIDI M., KOENDERINK J. J.: Diffuse and specular reflectance from rough surfaces. *Appl. Opt. 37*, 1 (1998), 130–139. URL: http://ao.osa.org/abstract.cfm?URI=ao-37-1-130. 2

[WJHY22] WANG B., JIN W., HAŠAN M., YAN L.-Q.: Spongecake: A layered microflake surface appearance model. *ACM Trans. Graph. 42*, 1 (Sept. 2022). URL: https://doi.org/10.1145/3546940, doi:10.1145/3546940. 2

[WMLT07] WALTER B., MARSCHNER S., LI H., TORRANCE K.: Microfacet models for refraction through rough surfaces. In *Rendering Techniques (Proc. EG Symposium on Rendering)* (2007), pp. 195–206. URL: https://dl.acm.org/doi/abs/10.5555/2383847.2383874. 2

[WNO98] WOLFF L. B., NAYAR S. K., OREN M.: Improved diffuse reflection models for computer vision. *International Journal of Computer Vision 30*, 1 (1998), 55–71. URL: https://doi.org/10.1023/A:1008017513536. 2

[ZJMB11] ZHAO S., JAKOB W., MARSCHNER S., BALA K.: Building volumetric appearance models of fabric using micro CT imaging. *ACM Trans. Graph. 30*, 4 (July 2011). URL: https://doi.org/10.1145/2010324.1964939, doi:10.1145/2010324.1964939. 2, 3

[ZRW*24] ZELTNER T., ROUSSELLE F., WEIDLICH A., CLARBERG P., NOVÁK J., BITTERLI B., EVANS A., DAVIDOVIČ T., KALLWEIT S., LEFOHN A.: Real-time neural appearance models. *ACM Trans. Graph.* (Apr. 2024). URL: https://doi.org/10.1145/3659577, doi:10.1145/3659577. 7